Title: Noncaloric monosaccharides induce excessive sprouting angiogenesis in zebrafish via foxo1a-marcksl1a signal

Running title: Noncaloric Monosaccharides Induce Excessive Angiogenesis

Xiaoning wang[1, *], Jinxiang Zhao[1, 2, *], Jiehuan Xu[3, *], Bowen Li[1], Xia Liu[3, #], Gangcai Xie[3, #], Xuchu Duan[1, #], Dong Liu[1, #]

1 Affiliated Hospital of Nantong University, Nantong Laboratory of Development and Diseases, School of Life Science; Co-innovation Center of Neuroregeneration, Nantong University, Nantong, China

2 Suqian First Hospital, Suqian, China

3 Medical School, Nantong University, Nantong, China

[*], These authors contributed equally to this work.

[#], Authors for correspondence:

Dong Liu, Ph.D

School of Life Sciences, Jiangsu Key Laboratory of Neuroregeneration, Nantong University

Building 15-C1213, Seyuan Road 9#, Nantong, China, 226001

Phone: + (86) - 18605133927

Fax: + (86) - 513 - 85511585

Email: liudongtom@gmail.com; tom@ntu.edu.cn

Abstract

Artificially sweetened beverages containing noncaloric monosaccharides were suggested as healthier alternatives to sugar-sweetened beverages. Nevertheless, the potential detrimental effects of these noncaloric monosaccharides on blood vessel function remain inadequately understood. We have established a zebrafish model that exhibits significant excessive angiogenesis induced by high glucose, resembling the hyperangiogenic characteristics observed in proliferative diabetic retinopathy (PDR). Utilizing this model, we observed that glucose and noncaloric monosaccharides could induce excessive formation of blood vessels, especially intersegmental vessels (ISVs). The excessively branched vessels were observed to be formed by ectopic activation of quiescent endothelial cells (ECs) into tip cells. Single-cell transcriptomic sequencing analysis of the endothelial cells in the embryos exposed to high glucose revealed an augmented ratio of capillary ECs, proliferating ECs, and a series of upregulated proangiogenic genes. Further analysis and experiments validated that reduced *foxo1a* mediated the excessive angiogenesis induced by monosaccharides via up-regulating the expression of *marcksl1a*. This study has provided new evidence showing the negative effects of noncaloric monosaccharides on the vascular system and the underlying mechanisms.

Key words: noncaloric monosaccharides; endothelial cell activation; *foxo1a*; *marcksl1a*; zebrafish

Introduction

Diabetes mellitus (DM) encompasses a group of chronic diseases characterized by elevated blood glucose levels. Among patients with DM, cardiovascular complications, especially the direct and indirect effects of hyperglycemia on the human vascular network, persist as the primary cause of morbidity and mortality [1]. The harmful effects of hyperglycemia are closely associated with both microvascular and macrovascular complications, including retinopathy, nephropathy, neuropathy, atherosclerosis, ischemic heart disease, stroke, and peripheral artery disease [2, 3]. Endothelial cell dysfunction (ECD) is a systemic pathological state exhibiting disrupted integrity, adhesion, altered proliferation capacity, migration, tube formation, and more [4, 5]. High blood glucose levels over long periods have been demonstrated to be associated with vascular dysfunction both *in vivo* and *in vitro* [6, 7].

The epidemiological evidence has indicated the positive correlation between risks of cardiovascular disease and DM with the consumption of sugar-sweetened beverages (SSBs) and 100% fruit juices, thereby emphasizing the concerns for the adverse effects of sugar intake on cardiometabolic risk factors, regardless of whether the sugar is added or naturally occurring [8-12]. Artificially sweetened beverages (ASBs), which incorporate noncaloric sweeteners or low-caloric additives, have been suggested as healthy alternatives to SSBs [13]. ASBs contain sugar alcohols and polyols, such as sorbitol, xylitol, maltitol, mannitol, erythritol, isomalt, and lactitol. The consumption of ASBs worldwide has gradually increased in recent years [13-15]. However, accumulating studies in the last decade suggested that ASB consumption might be associated with an increased risk of cardiovascular events and diabetes

[12, 16-23]. Nevertheless, the underlying mechanisms responsible for these findings remain insufficiently documented.

The zebrafish has been recognized as a valuable animal model for studying metabolic diseases, such as hyperglycemia and diabetic complications, due to its functional conservation in glycol metabolism, pancreas structure, glucose homeostasis, adipose biology, and genetic similarities to mammals [24-26]. The combination of embryonic transparency and transgenic lines, wherein endothelial cells are labeled specifically with fluorescent proteins, facilitates the high-resolution imaging analysis of vascular formation *in vivo*. Immersion of zebrafish in glucose solution has been found to induce diabetic complications, including vascular dysfunction [27-30]. Several recent studies have investigated the effects of high glucose on vascular function in the zebrafish model [30-32]. However, the association between noncaloric monosaccharides and vascular dysfunctions, such as excessive angiogenesis, has not been elucidated. Here, we have successfully established a short-term zebrafish model that exhibits significantly excessive angiogenesis similar to the phenotypes observed in proliferative diabetic retinopathy (PDR) induced by glucose treatment. Using this model, we examined the effects of noncaloric monosaccharides on blood vessel development and investigated the molecular mechanisms. Our results provided new evidence for the negative roles of caloric and noncaloric monosaccharides on vascular development.

Results

Establishment of a short-term model of high-glucose-induced excessive angiogenesis

To establish the short-term zebrafish hyperangiogenenic model induced by high-glucose treatment, we immersed the *Tg(fli1aEP:EGFP-CAAX)*^{ntu666} embryos, a transgenic line wherein the endothelial cells were labeled with membrane-bound GFP (Supplementary Figure 1), in glucose solution within a wide range of concentrations and time windows (Supplementary Figure 2). We subsequently measured the glucose concentration in the embryos. We found that the glucose concentration in the embryos treated with high glucose was significantly higher than that in the control group (Supplementary Figure 3). We observed that exposing zebrafish embryos at either 24 hours post fertilization (hpf) or 48 hpf to a 6% D-glucose treatment for a duration exceeding 48 hours led to dramatically increased formation of blood vessels (Figure 1, Movie 1 and 2), especially intersegmental vessels (ISVs) in the indicated area (Figure 1b). The hyperbranched endothelial cells were observed to sprout from existing vessels, including the ISVs, dorsal aorta (DA), and dorsal lateral anastomotic vessel (DLAV) (Figure 1) in embryos treated with high glucose.

Additionally, these ectopically branched angiogenic sprouts were not perfused by blood flow. Despite the abnormal vessel formation, no significant developmental defects were observed in these treated embryos when examined under a bright field microscope (Supplementary Figure 4a-c). Moreover, no excessive angiogenic phenotype was observed in the embryos treated with 1%, 2%, 3%, and 4% D-glucose within the corresponding time frame (Supplementary Figure 5).

Fructose and noncaloric monosaccharides induce excessive angiogenesis

Fructose is a ketonic monosaccharide that is an energy source for living organisms. Therefore, our study investigated the potential effects of fructose on vascular dysfunction in comparison to glucose. The result demonstrated fructose-induced excessive angiogenesis in zebrafish embryos (Supplementary Figure 6). Wondering whether the effects of glucose and fructose on vascular development were mediated by metabolic events, we then conducted the same tests by using other noncaloric monosaccharides, including L-glucose, D-mannose, D-ribose, and L-arabinose, which animals could not digest. Interestingly, we observed that all these noncaloric monosaccharides could induce excessive angiogenesis, among which the L-glucose purchased from two companies resulted in a similar phenotype as efficiently as D-glucose did (Figure 2a-h). To rule out the effect of osmotic pressure, we treated zebrafish embryos with isotonic disaccharides, including lactose, maltose, and sucrose, which did not cause a significant excessive angiogenic phenotype (Supplementary Figure 4d, h; Supplementary Figure 7). However, higher concentration disaccharide treatment can also cause excessive angiogenesis in zebrafish embryos (Supplementary Figure 8). In addition, we also tested the effects of pyruvic acid but did not observe the excessive angiogenic phenotype in the embryos treated with pyruvic acid solution at 50 nM~50 μM concentration (Supplementary Figure 9). Furthermore, we examined the arterial and venous identity of the hyperbranched vessels via live imaging analysis of the high glucose-treated *Tg(flt1:YFP::kdrl:ras-mCherry)* line, in which the YFP expression in the artery was relatively higher than that in the vein [33]. The result revealed that the hyperbranched ectopic vessels comprised arteries and veins (Figure 2i, j).

High glucose promotes quiescent endothelial differentiation into tip cells

Given that a high-glucose shock has been observed to induce excessive angiogenesis in 48 hpf embryos, it was hypothesized that the shock might play a crucial role in regulating the differentiation of quiescent endothelial cells (ECs) into active tip cell-like cells and their subsequent behaviors. To investigate whether this was the case, we observed the behaviors of these ECs by confocal time-lapse imaging analysis. As shown in the result, in control *Tg(fli1aEP:EGFP-CAAX)*^{ntu666} embryos, no significant activation of tip cells in the angiogenic sprouts was observed in the generated ISVs, DA, and DLAV in the embryos aged from 48 hpf to 5 dpf. Moreover, only a few ECs in established ISVs, DA, and DLAV extended filopodia, which quickly retracted (Figure 3a-c, Movie 3). However, many ECs initiated sprouting angiogenesis in the high glucose-treated embryos, extended dynamic filopodia to sense the surroundings, and formed excessive ectopic blood vessels (Figure 3d-e, Movie 4). In a snapshot, we observed that some of the ECs protruded long and intricate sprouts simultaneously (Figure 3f), and nearly all the ECs within an ISV underwent the outgrowth of filopodia in some extreme cases (Figure 3g), suggesting that the high glucose treatment induced the endothelial differentiation into tip cell-like cells. Furthermore, we observed that these outgrowths of the ectopic angiogenic sprouts could establish a connection to the neighboring sprouts and vessels and thereby form complicated vascular structures (Figure 1c, f, i, l, p).

Single-cell transcriptomic sequencing analysis of the endothelial cells isolated from glucose-treated embryos

We did a single-cell transcriptomic sequencing analysis to gain more insight into the potential mechanism through which glucose activates the endothelial cells. Due to the limited presence of endothelial cells within the zebrafish embryos, the analysis of these cells poses a challenge. Firstly, we isolated the EGFP-positive cells from control and high glucose-treated embryos. Following the proteolytic dissociation of embryos, the EGFP-positive cells were isolated by fluorescence-activated cell sorting (FACS). Around 300-500 zebrafish embryos were used for the ECs collection for each stage. The isolated ECs were analyzed using a large-scale scRNA-seq (10X Genomics) platform, and the pipeline is illustrated in the diagram (Figure 4a). Multiple criteria were applied to select the single cells, including the retention of the genes that were expressed (Unique Molecular Identifiers or UMI larger than 0) in at least 3 individual cells, the selection of cells with the gene expression count falling within the range of 500 to 3000, and the imposition of a threshold wherein the proportion of sequencing reads derived from the mitochondrial genome was limited to less than 5% (Supplementary Figure 10, Supplementary Figure 11, Supplementary Table 1). Ultimately, 6006 endothelial cells were selected for further analysis (Supplementary Table 2).

Through clustering analysis of gene expression, these ECs were categorized into 6 clusters using UMAP. These clusters include cluster 0, which consists of arterial and capillary ECs; cluster1, comprising endocardium; cluster2, consisting of venous and lymphatic ECs; cluster3, comprising arch ECs; cluster4, encompassing proliferating ECs; and cluster5, consisting of vesicle enriched ECs (Figure 4b). The endothelial marker gene *cdh5* was expressed in all the clusters (Figure 4c). The notch ligand *dlc* was highly expressed in arterial,

capillary ECs, and arch ECs (Figure 4d). The *dab2* and *prox1* were mainly enriched in venous and lymphatic ECs (Figure 4e-f). The *cdk1*, a key player in cell cycle regulation, was specifically expressed in proliferating ECs (Figure 4h). It was revealed that the ratio of arterial and capillary ECs and proliferating ECs was increased in the high glucose-treated embryos (Figure 4i, j), consistent with the observation that glucose treatment resulted in excessive sprouting angiogenesis of ISVs. In addition, we examined tip cell marker genes in arterial and capillary ECs. The results showed that the expression of *esm1*, *cxcr4a*, and *apln* was significantly up-regulated after high glucose treatment (Figure 3h-k), consistent with our observation that high glucose treatment induced the endothelial differentiation into tip cell-like cells (Figure 3f, g).

We also performed the whole embryo transcriptome sequencing after high D-glucose and L-glucose treatment. We analyzed and compared the differentially expressed genes of control, high D-glucose-treated, and high L-glucose-treated embryos. The results revealed that 1259 and 1074 genes were up-regulated significantly in high D-glucose and high L-glucose treated embryos, respectively, compared with the control (Supplementary Figure 12). After that, we analyzed the expression of the genes related to metabolic pathways and found significant alteration in the expression of several genes involved in Gluconeogenesis, Glycolysis, and Oxidative phosphorylation (Supplementary Figure 13).

Foxo1a was significantly downregulated in arterial and capillary ECs

To identify the potential molecules responsible for increasing the proportion of arterial and capillary ECs in the embryos treated with glucose, we analyzed and compared the

differentially expressed genes (DEGs) in arterial and capillary ECs of control and glucose-treated ECs. The results revealed that 1201 genes were up-regulated and 523 genes were down-regulated significantly (Figure 5a). GO analysis revealed that these DEGs were enriched in several biological processes, including regulation of actin filament organization, blood vessel morphogenesis, development, angiogenesis, etc. (Figure 5b).

Subsequently, we searched for transcription factors among the genes involved in the aforementioned biological processes that might participate in inducing excessive angiogenesis. It has been reported that the loss of function of *foxo1a* led to excessive angiogenesis [34, 35]. Our study also revealed that *foxo1a* was significantly downregulated in arterial and capillary ECs after high glucose treatment compared to the ECs marker gene *pecam1*(Figure 5c-e). The *in situ* hybridization (ISH) experiments further confirmed the decrease in *foxo1a* expression following treatment with high D-glucose and L-glucose (Figure 5f). To verify whether the downregulation of Foxo1a led to excessive angiogenesis in zebrafish embryos, we performed loss-of-function experiments targeting *foxo1a*. AS1842856, a cell-permeable inhibitor reported to block *FOXO1* transcription activity [36], was administered to zebrafish embryos at 48 hpf, and the imaging was performed at 72 hpf. The results revealed significantly excessive angiogenesis in AS1842856 treated embryos compared with the control group, consistent with the results obtained from *foxo1a* MO injection (Figure 5g-i).

To further validate that the excessive angiogenesis induced by high glucose was attributed to Foxo1a deficiency, we performed rescue experiments. In detail, *foxo1a* was overexpressed

in either whole embryos or ECs, driven by *hsp70l* and *fli1EP* promoter, respectively. We injected the overexpression construct into one-cell stage embryos followed by heat shock at 24 hpf and 48 hpf. The embryos were then treated with high glucose from 48 hpf to 96 hpf (Figure 6a). The results indicated that the gain of function of foxo1a in either whole embryos or ECs significantly and partially mitigated the excessive angiogenesis induced by high glucose treatment (Figure 6b-j).

Monosaccharides induced excessive angiogenesis through the *foxo1a-marcksl1a* pathway.

A previous study has reported that *marcksl1a* overexpression in ECs in zebrafish led to a significant increase in filopodia formation, similar to the phenotype we observed in response to high glucose treatment [37]. Our analysis of the single-cell sequencing data revealed a significant upregulation of *marcksl1a* in arterial and capillary ECs following high glucose treatment, compared to the ECs marker gene *kdrl* (Figure 7a, b). The real-time qPCR and ISH experiments further confirmed the elevated expression levels of *marcksl1a* following high D-glucose and L-glucose treatment (Figure 7c, d). Then, by constructing the transgenic zebrafish line *hsp70l:marcksl1a-p2A-mCherry:: Tg(fli1a:EGFP-CAAX)* ^{ntu666}, we conducted the experiments to overexpress *marcksl1a* in zebrafish and subsequently observed the vascular developmental phenotype. After one hour of heat shock at 24 hpf and confocal imaging analysis at 72 hpf, significantly increased blood vessel formation was observed in embryos overexpressing *marcksl1a*, compared with the control group (Figure 7e-g).

Given the results obtained from *marcksl1a* overexpression and loss of function of *foxo1a*, we hypothesized that *marcksl1a* might be a target gene of Foxo1a. Therefore, we investigated

the impact of Foxo1 inhibition on *marcksl1a* expression in zebrafish embryos. As expected, qPCR analysis revealed that inhibition of Foxo1a by AS1842856 resulted in the upregulation of marcksl1a expression. In contrast, Foxo1a overexpression resulted in the downregulation of *marcksl1a* (Figure 8a-c), which suggested that Foxo1a might negatively regulate *marcksl1a* transcription in zebrafish. To further confirm it, we performed the Chromatin Immunoprecipitation (ChIP) experiment to validate the potential binding interaction between Foxo1 and *marcksl1a*. Since the amino acid sequence and DNA binding motifs of Foxo1 are highly conserved between zebrafish and mice (Supplementary Figure 14), we analyzed the 3 kb promoter region of *marcksl1a* to search the binding site sequence of mouse FOXO1 presented in the JASPAR database. Two candidate binding sites (BS) were found at −265 to −275 (BS1) and −153 to −163 (BS2) nucleotides upstream of the TSS of *marcksl1a* (Figure 8d) and then used for the ChIP-PCR assay detection. The results showed that Foxo1a was enriched in both the predicted binding sites of *marcksl1a* (Figure 8e) in zebrafish. Luciferase reporter assay also indicated that Foxo1a could negatively regulate marcksl1a transcription in zebrafish (Figure 8f, g).

Additionally, we microinjected *marcksl1a* MO into the 1-cell stage *Tg(fli1a:EGFP-CAAX)*^{ntu666} embryos, which were then treated with high levels of D-glucose and L-glucose. The findings revealed that the knockdown of Marcksl1a could effectively mitigate the excessive angiogenesis caused by high D-glucose or high L-glucose treatment, resembling the rescue effect observed with VEGFR inhibitor Lenvatinib (Figure 8h-n, Supplementary Figure 15). These results suggested that monosaccharides induced excessive angiogenesis through the

Foxo1a-*marcksl1a* pathway in zebrafish embryos.

Discussion

In this study, we successfully established a new zebrafish model with significant excessive angiogenesis, resembling the hyperangiogenic characteristics observed in PDR more closely than previously established models [30, 32]. Seung-Hyun Jung et al. have described a short-term zebrafish model for diabetic retinopathy (DR) induced by high glucose, which exhibited blood vessel defects[30]. However, these defects were limited to the disruption of tight junctions and dilation of hyaloid-retinal vessels [30], without the excessive angiogenesis and vascular blockage observed in PDR and our established model. Additionally, although Kristina Jörgens et al. have observed the hyperbranching of small vessel structures originating from the upper part of ISVs, growing horizontally towards and partially connecting to the neighboring ISVs Field [32], the angiogenic sprouts did not form a more complex structure that was observed in our research.

The excessive development of immature blood vessels represents a significant pathological condition in the progression of DR and nephropathy [38, 39]. Hyperglycemia has been considered one of the most causal factors causing vascular damage, including excessive angiogenesis. However, the exact mechanism through which hyperglycemia impairs the blood vessels is not well determined. We analyzed single-cell transcriptomic sequencing data of the endothelial cells isolated from D-glucose-treated embryos to gain more insights into it. The findings revealed an increased ratio of tip cells and proliferating ECs, accompanied by the altered expression of various angiogenic genes in the ECs of D-glucose-treated embryos.

Foxo1 has been validated to be essential for sustaining the quiescence of endothelial cells,

with involvement in metabolism regulation [34, 40]. Moreover, it also plays an important role in diabetic microvascular complications, including DR[41, 42]. Here, by combining the single-cell transcriptomic sequencing data analysis and experimental validation, we identified the transcription factor Foxo1a, which was significantly down-regulated in the embryos treated with high glucose, responsible for the excessive angiogenesis. Additionally, our result further revealed that Foxo1a exerts its regulatory function during this process by down-regulating its target gene *marcksl1a*, regardless of whether the embryos were treated with D-glucose or L-glucose. Taken together, our results suggested that both caloric and noncaloric monosaccharides treatment could lead to excessive angiogenesis by promoting the differentiation of quiescent endothelial cells into tip cells through the *foxo1a-marcksl1a* pathway.

Previous studies have linked the consumption of ASB to the occurrence and development of cardiovascular disease [12, 16-23]. However, the potential mechanisms underlying the association have not been well documented. In recent years, positive associations between ASB and cardiovascular disease have been proposed, possibly due to several plausible factors, including the potential impact of ASBs on central nervous system circuits, gut hormone secretion, and gut microbiota [43-45]. Additionally, it has been hypothesized that the ASBs might stimulate appetite and increase calorie intake [43, 44].

For a long time, there has been considerable debate and conflicting opinions regarding how specific sugars affect the development of type 2 diabetes rather than excess calories per se [46, 47]. In this study, we have provided new evidence indicating that the administration of

noncaloric monosaccharides leads to significant excessive angiogenesis, suggesting that the excessive angiogenesis may not be only attributed to the caloric properties. Since excessive angiogenesis is the major pathological feature of diabetic retinopathy and nephropathy, our findings are in support of a possible biological mechanism underlying the positive associations between noncaloric monosaccharides and microvascular complications associated with type 2 diabetes, suggesting that the noncaloric monosaccharides might not be suitable for ASB consumption.

Surprisingly, no notable abnormalities were observed in the vessels of embryos treated with disaccharides, including lactose, maltose, and sucrose, which is consistent with the previous study stating that intakes of sucrose, lactose, and maltose were not significantly associated with the risk of type 2 diabetes [48]. This finding implied that the effects induced by monosaccharides cannot be attributed to the osmotic pressure of the surrounding medium. Furthermore, despite the potential conversion of these disaccharides into monosaccharides, the restricted reaction rate may maintain them within a safe concentration range that is not harmful to the vessels in a short period.

In conclusion, to investigate the effects of monosaccharides on vascular development, we established a zebrafish model by treating the embryos with high concentrations of monosaccharides. Based on this model, we observed significant excessive angiogenesis induced by glucose and noncaloric monosaccharides, initiated by activating the quiescent endothelial cells into proliferating tip cells. The effects of monosaccharides on inducing excessive angiogenesis were then proved to be mediated by the *foxo1a-marcksl1a* pathway.

The results have provided novel insights into the roles of noncaloric monosaccharides in human health and the underlying mechanisms.

Materials and methods

Zebrafish

Care and breeding of zebrafish were carried out as previously described [49]. Animal experiments were conducted according to local institutional laws and Chinese law for the Protection of Animals. The following transgenic strains were used: *Tg(fli1aEP:EGFP-CAAX)*^{ntu666} and *Tg(kdrl:ras-mCHerry* [33]. Embryos were obtained through natural mating and maintained at 28.5°C. The stages of zebrafish embryos are defined as previously described [49]. Embryos were treated with 0.2 mM 1-phenyl-2-thiourea (PTU, Sigma, P7629) to block pigmentation for further imaging analysis.

Monosaccharides and drug treatment

The D-glucose (Sigma, G7021-100g), L-glucose (Sigma, G5500-1g; J&K, 981195-1g), D-Fructose (Sigma, F0127-100g), L-Rhamnose monohydrate (Aladdin, R108982), D-Sorbitol (Sigma, S1876-100g), D-Mannitol (Sigma, M4125-100g), D-(-)-Ribose (Sigma, V900389-25g), L-(+)-Arabinos (Sigma, V900920-25g), Mannose (Sigma, M2069-25g) and sucrose (Sigma, V900116-500G) were dissolved in E3 solution. Zebrafish embryos at 24 hpf to 48 hpf were placed in 24-well plates (ten embryos per well) and immersed in the solution at the presetting concentrations and time windows. Then, put it in a 28 □ incubator for cultivation. Five days before embryonic development, a stereo fluorescence microscope and a laser confocal microscope were used to observe the changes in blood vessel phenotype. For the

drug treatment, the embryos were co-incubated in glucose with Lenvatinib (Selleck, S1164-5MG) at the presetting concentrations and time window. Foxo1 inhibitor AS1842856 (MCE, HY-100596) was dissolved in DMSO and stored at -80□ and diluted with E3 solution to 1 μM when used. The same concentration of DMSO was used as a negative control.

Glucose concentration measurement

Glucose concentration in the embryo was measured as described previously [50]. Embryos that developed to 75% epiboly were selected and transferred to 24-well plates (ten embryos per well) and immersed in the solution at the presetting concentrations and time windows. For glucose concentration measurement, embryos (n=20) were transferred to a new 1.5 mL tube, rinsed three times with 1×PBS, and immersed in ice for the following experiments. Discard the PBS as much as possible, embryos homogenized using a hand homogenizer, and centrifuged at 14,000×g for 10 min. 1.5 μL of the supernatant was used to measure the total free-glucose level using a glucometer (Baye, 7600P).

Whole-mount in situ hybridization (WISH)

Whole-mount in situ hybridization and the preparation of antisense RNA probes were performed as described in the previous protocol [51]. Briefly, the *marcksl1a* and *foxo1a* cDNA fragments were cloned with the specific primers listed below using the wild-type embryo (AB) cDNA library. Probes were synthesized using the in vitro DIG-RNA labeling transcription Kit (Roche, 11175025910) with linearized pGEM-T easy vector containing *marcksl1a* or *foxo1a* gene fragment as the templates. Synthesized probes were purified with LiCl (Invitrogen, AM9480) and diluted to 1 ng/μL for hybridization. Zebrafish embryos were

collected and fixed with 4% paraformaldehyde (PFA) overnight at 4˚C, then dehydrated with methanol gradients and stored at -20□ in 100% methanol. The hybridization result was detected with anti-DIG-AP antibody (1:2000, Roche, 11093274910) and NBT/BCIP (1:500, Roche, 11681451001). After hybridization, images of the embryos were captured with an Olympus stereomicroscope MVX10. The primers are listed below:

marcksl1a-probe-forward:5'- AGG ATG GGT GCT CAG TTG AC-3'

marcksl1a-probe-reverse:5'- GCT GGC GTC TCA TTG GTT TC-3'

foxo1a-probe-forward:5'-GCA ACA CAG GAT TTC CCC AC-3'

foxo1a-probe-reverse:5'-CAC AGG TGG CAC TGG AAG G-3'

Single-cell gene expression profile analysis

Cell Ranger 3.0.2 (https://github.com/10XGenomics/cellranger) was used to convert the raw sequencing data to a single-cell level gene count matrix. The clustering of single cells and the marker genes in each cluster were analyzed by Seurat 3.0 (https://satijalab.org/seurat/install.html) [52]. Several criteria were applied to select the single cells, including only keeping the genes that are expressed (Unique Molecular Identifiers or UMI larger than 0) at least in 3 single cells, selecting single cells with the number of expressed genes at the range between 500 and 3000, and requiring the percentage of sequencing reads on mitochondrial genome being less than 5 percentage. Furthermore, sctransform method [53] was applied to remove technical variation, and ClusterProfiler [54] was used to do the Gene Ontology enrichment analysis based on the marker genes of each cell cluster. Detailed information about the data processing can be found in this project's

source code (https://github.com/gangcai/ZebEndoimmune).

Gene expression analysis by quantitative real-time PCR

Total RNA was extracted from zebrafish embryos using TRIzol™ (Invitrogen, 15596026), and stored at -80□. The cDNA was then synthesized using the HiScript II Q RT SuperMix for qPCR Kit (Vazyme, R223-01) according to the manufacturer's instructions. Quantitative PCR was performed in triplicates using the Taq Pro Universal SYBR qPCR Master Mix (Vazyme, Q712-02) on a real-time PCR detection system (StepOne™ Real-Time PCR Systems). The primers used for Real-time PCR analysis are as follows:

ef1α-Qpcr-F:5'- CTT CAA CGC TCA GGT CAT CA -3'

ef1α-Qpcr-R:5'- CGG TCG ATC TTC TCC TTG AG -3

marcksl1a-Qpcr-F:5'- CCG TGG CTG ATA AAG CCA AT -3'

marcksl1a-Qpcr-R:5'- CTC CCT CCT CCG TTT TTG GG -3'

Transgenic and heat shock

The *Tg(fli1aEP:EGFP-CAAX)*^{ntu666} line was established using a construct *fli1aEP:EGFP-CAAX*, which was generated using multisite Gateway technology, the tol2 kit as previously described [55]. The 5' Entry p5Efli1ep (#31160) purchased from Addgene was originally from Nathan Lawson Lab [56]. Three entry clones and the pDestTol2pA2 destination vector were used to generate the expression construct by LR recombination reaction as described in the Multisite Gateway Manual book. The expression constructs were synthesized by GENEWIZ company. The zebrafish embryos were immersed in a 37 □ water bath for 1 hour for heat shock. Around 75 pg of expression plasmid DNA and 25 pg tol2 transposase mRNA

were premixed and microinjected into single-cell fertilized eggs.

Chip-PCR

Embryos injected with *hsp70l:foxo1a-6×His-P2A-mCherry* were collected at 72 hpf after heat shock treatment. According to the manufacturer's instructions, the ChIP-PCR assay was performed using the Chromatin Immunoprecipitation (ChIP) Assay Kit (Millipore, 3753379). The genomic DNA crossed with Foxo1a protein was immunoprecipitated by using 5 μg Anti-6×His tag antibody (abcam, ab213204). Antibody against lgG was used as a negative control. The semiquantitative PCR was performed with KODfx (TOYOBO, KFX-101) at the following conditions: 94□ for 5 min; 35 cycles of 98□ for 10 s, 55□ for 30 s, 68□ for 10 s; 68□ for 10 min. The PCR primers used for the predicted binding sites (BS) are as follows:

marcksl1a-BS1-forward:5'- CCC TTT TTC AAA AGT GAG TTT GAG -3'

marcksl1a -BS1-reverse:5'- GGA GCT TCA TCT GCC CCA TT -3'

marcksl1a -BS2-forward:5'- CGG TTT CCA GCT TTC TTC AGA A -3'

marcksl1a -BS2-reverse:5'- TCT CAA ACT CAC TTT TGA AAA AGG G -3'

Luciferase reporter assay

Plasmids of PGL4.10[luc2] and PGL4.74[hRluc/TK] (Promega) were used for luciferase reporter assay. Zebrafish *marcksl1a* promoter fragment with predictive Foxo1a binding cite was cloned and inserted into pGL4.10 basic vector by Kpn I and Hind III. The assays for detecting the promoter activity in response to Foxo1a were performed according to the previous study. Briefly, 50 pg of PGL4.10 vectors, 1 pg of PGL4.74 vectors, and 50 pg of *foxo1a* mRNA or 20 pg of *foxo1a* MO were co-injected into wild-type embryos at the one-

cell stage. And then, embryos were harvested at 24 hpf to measure their luciferase activity according to the manufacturer's protocols (Promega).

Imaging analysis

For confocal imaging of blood vessels in fluorescence protein labeled transgenic zebrafish embryos, they were anesthetized with egg water/0.16 mg/mL MS222 (Sigma, A5040)/1% PTU and embedded in 0.5-0.8% low melting agarose. Confocal imaging was performed with a Nikon A1R HD25 Confocal Microscope. Analysis was performed using Nikon-NIS-Elements software. The bright field images were acquired with an Olympus DP71 camera on an Olympus stereomicroscope MVX10.

Statistical analysis

Statistical analysis was performed with a student's *t-test*. All data is presented as Mean ± SEM; $p < 0.05$ was considered statistically significant.

Funding

This study was supported by grants from the National Natural Science Foundation of China (81870359, 2018YFA0801004).

Conflicts of interest/Competing interests

The authors declare that they have no conflicts of interest

Availability of data and material (data transparency)

All the experimental materials generated in this study are available from the corresponding authors upon reasonable request.

Authors' contributions

Dong Liu, Xuchu Duan, Xia Liu, and Gangcai Xie conceived and designed the experiments and wrote the manuscript. Xiaoning wang, Jinxiang Zhao, Jiehuan Xu, Bowen Li, and Gangcai Xie performed the experiments and analyzed the data. All authors read and approved the final manuscript.

Ethics approval

All zebrafish experimentation was carried out following the NIH Guidelines for the care and use of laboratory animals (http://oacu.od.nih.gov/regs/index.htm) and ethically approved by the Administration Committee of Experimental Animals, Jiangsu Province, China (Approval ID: 20180905-002).

Acknowledgments

Not applicable

Reference

1. Matheus, A.S., et al., *Impact of diabetes on cardiovascular disease: an update.* Int J Hypertens, 2013. **2013**: p. 653789.
2. Fox, C.S., et al., *Trends in cardiovascular complications of diabetes.* JAMA, 2004. **292**(20): p. 2495-9.
3. Rask-Madsen, C. and G.L. King, *Vascular complications of diabetes: mechanisms of injury and protective factors.* Cell Metab, 2013. **17**(1): p. 20-33.
4. Flammer, A.J., et al., *The assessment of endothelial function: from research into clinical practice.* Circulation, 2012. **126**(6): p. 753-67.
5. Kolluru, G.K., S.C. Bir, and C.G. Kevil, *Endothelial dysfunction and diabetes: effects on angiogenesis, vascular remodeling, and wound healing.* Int J Vasc Med, 2012. **2012**: p. 918267.
6. Tesfamariam, B., et al., *Elevated glucose promotes generation of endothelium-derived vasoconstrictor prostanoids in rabbit aorta.* J Clin Invest, 1990. **85**(3): p. 929-32.
7. Ting, H.H., et al., *Vitamin C improves endothelium-dependent vasodilation in patients with non-insulin-dependent diabetes mellitus.* J Clin Invest, 1996. **97**(1): p. 22-8.
8. Imamura, F., et al., *Consumption of sugar sweetened beverages, artificially sweetened beverages, and fruit juice and incidence of type 2 diabetes: systematic review, meta-analysis, and estimation of population attributable fraction.* BMJ, 2015. **351**: p. h3576.
9. Malik, V.S., *Sugar sweetened beverages and cardiometabolic health.* Curr Opin Cardiol, 2017. **32**(5): p. 572-579.
10. Narain, A., C.S. Kwok, and M.A. Mamas, *Soft drinks and sweetened beverages and the risk of cardiovascular disease and mortality: a systematic review and meta-analysis.* Int J Clin Pract, 2016. **70**(10): p. 791-805.
11. Larsson, S.C., A. Akesson, and A. Wolk, *Sweetened beverage consumption is associated with increased risk of stroke in women and men.* J Nutr, 2014. **144**(6): p. 856-60.
12. Fung, T.T., et al., *Sweetened beverage consumption and risk of coronary heart disease in women.* Am J Clin Nutr, 2009. **89**(4): p. 1037-42.

13. Fakhouri, T.H., B.K. Kit, and C.L. Ogden, *Consumption of diet drinks in the United States, 20092010.* NCHS Data Brief, 2012(109): p. 1-8.
14. Sylvetsky, A.C., et al., *Low-calorie sweetener consumption is increasing in the United States.* Am J Clin Nutr, 2012. **96**(3): p. 640-6.
15. Moriconi, E., et al., *Neuroendocrine and Metabolic Effects of Low-Calorie and Non-Calorie Sweeteners.* Front Endocrinol (Lausanne), 2020. **11**: p. 444.
16. de Koning, L., et al., *Sweetened beverage consumption, incident coronary heart disease, and biomarkers of risk in men.* Circulation, 2012. **125**(14): p. 1735-41, S1.
17. Fagherazzi, G., et al., *Consumption of artificially and sugar-sweetened beverages and incident type 2 diabetes in the Etude Epidemiologique aupres des femmes de la Mutuelle Generale de l'Education Nationale-European Prospective Investigation into Cancer and Nutrition cohort.* Am J Clin Nutr, 2013. **97**(3): p. 517-23.
18. Gardener, H., et al., *Diet soft drink consumption is associated with an increased risk of vascular events in the Northern Manhattan Study.* J Gen Intern Med, 2012. **27**(9): p. 1120-6.
19. Drouin-Chartier, J.P., et al., *Changes in Consumption of Sugary Beverages and Artificially Sweetened Beverages and Subsequent Risk of Type 2 Diabetes: Results From Three Large Prospective U.S. Cohorts of Women and Men.* Diabetes Care, 2019. **42**(12): p. 2181-2189.
20. de Koning, L., et al., *Sugar-sweetened and artificially sweetened beverage consumption and risk of type 2 diabetes in men.* Am J Clin Nutr, 2011. **93**(6): p. 1321-7.
21. Hirahatake, K.M., et al., *Cumulative intake of artificially sweetened and sugar-sweetened beverages and risk of incident type 2 diabetes in young adults: the Coronary Artery Risk Development In Young Adults (CARDIA) Study.* Am J Clin Nutr, 2019. **110**(3): p. 733-741.
22. Mossavar-Rahmani, Y., et al., *Artificially Sweetened Beverages and Stroke, Coronary Heart Disease, and All-Cause Mortality in the Women's Health Initiative.* Stroke, 2019. **50**(3): p. 555-562.
23. Vyas, A., et al., *Diet drink consumption and the risk of cardiovascular events: a report from the Women's Health Initiative.* J Gen Intern Med, 2015. **30**(4): p.

522 462-8.
523 24. Zang, L., L.A. Maddison, and W. Chen, *Zebrafish as a Model for Obesity and*
524 *Diabetes.* Front Cell Dev Biol, 2018. **6**: p. 91.
525 25. Barros, T.P., et al., *Zebrafish: an emerging technology for in vivo*
526 *pharmacological assessment to identify potential safety liabilities in early drug*
527 *discovery.* Br J Pharmacol, 2008. **154**(7): p. 1400-13.
528 26. Elo, B., et al., *Larval zebrafish as a model for glucose metabolism: expression*
529 *of phosphoenolpyruvate carboxykinase as a marker for exposure to anti-*
530 *diabetic compounds.* J Mol Endocrinol, 2007. **38**(4): p. 433-40.
531 27. Gleeson, M., V. Connaughton, and L.S. Arneson, *Induction of hyperglycaemia*
532 *in zebrafish (Danio rerio) leads to morphological changes in the retina.* Acta
533 Diabetol, 2007. **44**(3): p. 157-63.
534 28. Alvarez, Y., et al., *Predominant cone photoreceptor dysfunction in a*
535 *hyperglycaemic model of non-proliferative diabetic retinopathy.* Dis Model
536 Mech, 2010. **3**(3-4): p. 236-45.
537 29. Jorgens, K., et al., *Zebrafish: a model for understanding diabetic*
538 *complications.* Exp Clin Endocrinol Diabetes, 2012. **120**(4): p. 186-7.
539 30. Jung, S.H., et al., *High glucose-induced changes in hyaloid-retinal vessels*
540 *during early ocular development of zebrafish: a short-term animal model of*
541 *diabetic retinopathy.* Br J Pharmacol, 2016. **173**(1): p. 15-26.
542 31. Heckler, K. and J. Kroll, *Zebrafish as a Model for the Study of Microvascular*
543 *Complications of Diabetes and Their Mechanisms.* Int J Mol Sci, 2017. **18**(9).
544 32. Jorgens, K., et al., *High tissue glucose alters intersomitic blood vessels in*
545 *zebrafish via methylglyoxal targeting the VEGF receptor signaling cascade.*
546 Diabetes, 2015. **64**(1): p. 213-25.
547 33. Krueger, J., et al., *Flt1 acts as a negative regulator of tip cell formation and*
548 *branching morphogenesis in the zebrafish embryo.* Development, 2011.
549 **138**(10): p. 2111-20.
550 34. Wilhelm, K., et al., *FOXO1 couples metabolic activity and growth state in the*
551 *vascular endothelium.* Nature, 2016. **529**(7585): p. 216-20.
552 35. Rudnicki, M., et al., *Endothelial-specific FoxO1 depletion prevents obesity-*
553 *related disorders by increasing vascular metabolism and growth.* Elife, 2018.
554 **7**.

555 36. Zhao, W., et al., *Endothelial CDS2 deficiency causes VEGFA-mediated*
556 *vascular regression and tumor inhibition.* Cell Res, 2019. **29**(11): p. 895-910.
557 37. Kondrychyn, I., et al., *Marcksl1 modulates endothelial cell mechanoresponse*
558 *to haemodynamic forces to control blood vessel shape and size.* Nature
559 Communications, 2020. **11**(1): p. 5476.
560 38. Wilkinson-Berka, J.L., *Vasoactive factors and diabetic retinopathy: vascular*
561 *endothelial growth factor, cycoloxygenase-2 and nitric oxide.* Curr Pharm Des,
562 2004. **10**(27): p. 3331-48.
563 39. Osterby, R. and G. Nyberg, *New vessel formation in the renal corpuscles in*
564 *advanced diabetic glomerulopathy.* J Diabet Complications, 1987. **1**(4): p.
565 122-7.
566 40. Andrade, J., et al., *Control of endothelial quiescence by FOXO-regulated*
567 *metabolites.* Nat Cell Biol, 2021. **23**(4): p. 413-423.
568 41. Parmar, U.M., et al., *Emerging links between FOXOs and diabetic*
569 *complications.* Eur J Pharmacol, 2023. **960**: p. 176089.
570 42. Behl, T., et al., *Mechanistic insights into the role of FOXO in diabetic*
571 *retinopathy.* Am J Transl Res, 2022. **14**(6): p. 3584-3602.
572 43. Blundell, J.E. and A.J. Hill, *Paradoxical effects of an intense sweetener*
573 *(aspartame) on appetite.* Lancet, 1986. **1**(8489): p. 1092-3.
574 44. Pepino, M.Y., *Metabolic effects of non-nutritive sweeteners.* Physiol Behav,
575 2015. **152**(Pt B): p. 450-5.
576 45. Nettleton, J.E., R.A. Reimer, and J. Shearer, *Reshaping the gut microbiota:*
577 *Impact of low calorie sweeteners and the link to insulin resistance?* Physiol
578 Behav, 2016. **164**(Pt B): p. 488-493.
579 46. Qi, X. and R.F. Tester, *Lactose, Maltose, and Sucrose in Health and Disease.*
580 Mol Nutr Food Res, 2020. **64**(8): p. e1901082.
581 47. Laville, M. and J.A. Nazare, *Diabetes, insulin resistance and sugars.* Obes
582 Rev, 2009. **10 Suppl 1**: p. 24-33.
583 48. Montonen, J., et al., *Consumption of Sweetened Beverages and Intakes of*
584 *Fructose and Glucose Predict Type 2 Diabetes Occurrence1.* The Journal of
585 Nutrition, 2007. **137**(6): p. 1447-1454.
586 49. Wang, X., et al., *MicroRNA-10a/10b represses a novel target gene mib1 to*
587 *regulate angiogenesis.* Cardiovasc Res, 2016. **110**(1): p. 140-50.

588 50. Da'as, S.I., et al., *The link between glycemic control measures and eye*
589 *microvascular complications in a clinical cohort of type 2 diabetes with*
590 *microRNA-223-3p signature.* J Transl Med, 2023. **21**(1): p. 171.
591 51. Huang, Y., et al., *Nonmuscle myosin II-B (myh10) expression analysis during*
592 *zebrafish embryonic development.* Gene Expr Patterns, 2013. **13**(7): p. 265-
593 270.
594 52. Butler, A., et al., *Integrating single-cell transcriptomic data across different*
595 *conditions, technologies, and species.* Nat Biotechnol, 2018. **36**(5): p. 411-
596 420.
597 53. Hafemeister, C. and R. Satija, *Normalization and variance stabilization of*
598 *single-cell RNA-seq data using regularized negative binomial regression.*
599 Genome Biol, 2019. **20**(1): p. 296.
600 54. Yu, G., et al., *clusterProfiler: an R package for comparing biological themes*
601 *among gene clusters.* OMICS, 2012. **16**(5): p. 284-7.
602 55. Kwan, K.M., et al., *The Tol2kit: a multisite gateway-based construction kit for*
603 *Tol2 transposon transgenesis constructs.* Dev Dyn, 2007. **236**(11): p. 3088-99.
604 56. Villefranc, J.A., J. Amigo, and N.D. Lawson, *Gateway compatible vectors for*
605 *analysis of gene function in the zebrafish.* Dev Dyn, 2007. **236**(11): p. 3077-87.

606

607

Figure Legends

Figure 1 Glucose treatment caused excessive angiogenesis in zebrafish. a, A diagram showing the glucose treatment time window and imaging time point. **b**, A diagram indicating the imaging positions of the zebrafish embryos. **c**, Confocal imaging analysis of the control and glucose-treated embryos. The red bar indicates position 1; the green bar indicates position 2. Arrowheads indicate the ectopic branching from the dorsal aorta. Stars indicate the ectopic vessels from ISVs and DLAVs. **d**, Statistical analysis of the total length of ISVs in control and glucose-treated embryos. *t-test*, ****$p<0.0001$. **e**, A diagram showing the glucose treatment time window and imaging time point. **f**, Confocal imaging analysis of the control and glucose-treated embryos. The red bar indicates position 1; the green bar indicates position 2. Arrowheads indicate the ectopic branching from the dorsal aorta. Stars indicate the ectopic vessels from ISVs and DLAVs. **g**, Statistical analysis of the total length of ISVs in control and glucose-treated embryos. *t-test*, ****$p<0.0001$. **h**, A diagram showing the glucose treatment time window and imaging time point. **i**, Confocal imaging analysis of the control and glucose-treated embryos. The red bar indicates position 1; the green bar indicates position 2. Arrowheads indicate the ectopic branching from the dorsal aorta. Stars indicate the ectopic vessels from ISVs and DLAVs. **j**, Statistical analysis of the total length of ISVs in control and glucose-treated embryos. *t-test*, ****$p<0.0001$. **k**, A diagram showing the glucose treatment time window and imaging time point. **l**, Confocal imaging analysis of the control and glucose-treated embryos. The red bar indicates position 1; the green bar indicates position 2. Arrowheads indicate the ectopic branching from the dorsal aorta. Stars indicate the ectopic vessels from ISVs and DLAVs. **m**, Statistical analysis of the total length of ISVs in

control and glucose-treated embryos. *t-test*, ****p<0.0001. **o**, A diagram showing the blood vessels in position 2 indicated in panel b of control embryos. **p**, A diagram showing the blood vessels in position 2 indicated in panel b of high glucose-treated embryos.

Figure 2 L-glucose and mannose treatment caused excessive angiogenesis as well. a, A diagram showing the monosaccharides treatment time window and imaging time point. **b**, A diagram indicating the imaging position of the zebrafish embryos. **c-g**, Confocal imaging analysis of the control and monosaccharides, including L-glucose, D-mannose, D-ribose, and L-arabinose, treated embryos. Arrowheads indicate the ectopic branching from the dorsal aorta. Stars indicate the ectopic vessels from ISVs. **h**, Statistical analysis of the total length of ISVs in control and monosaccharides treated embryos. **i-j,** Confocal imaging analysis of the control and glucose-treated embryos. Arrowheads indicate the ectopic branching of arteries. Stars indicate the ectopic branching of veins. *t-test*, ****p<0.0001.

Figure 3 High glucose treatment induced endothelial differentiation into tip cell-like cells. a, A diagram showing the confocal time-lapse imaging time window. **b**, A diagram indicating the imaging position of the zebrafish embryos. **c,** Confocal time-lapse imaging analysis of blood vessels in control *Tg(fli1aEP:EGFP-CAAX)*^{ntu666} embryos. **d**, A diagram showing the glucose treatment time window and confocal time-lapse imaging time window. **e**, Confocal time-lapse imaging analysis of blood vessels in glucose-treated *Tg(fli1aEP:EGFP-CAAX)*^{ntu666} embryos. Arrowheads indicate the ectopic angiogenic branches. **f**, A snapshot of confocal time-lapse imaging analysis of blood vessels in glucose-treated *Tg(fli1aEP:EGFP-*

CAAX)^{ntu666} embryos. Z stacks were used to make 3D color projections, where blue represents the most proximal (closest to the viewer), and red represents the most distal (farthest from the viewer). Arrowheads indicate ectopic angiogenic sprouts. **g**, A snapshot of confocal time-lapse imaging analysis of an ISV in glucose-treated *Tg(fli1aEP:EGFP-CAAX)*^{ntu666} embryos. Arrowheads indicate ectopic angiogenic sprouts.

Figure 4 Single-cell transcriptome sequencing analysis of endothelial cells in control and high glucose treated embryos. a, Schematic diagram of the single-cell sequencing process. 300 embryos in the control group and 300 in the high glucose group were used, and ECs were sorted by GFP fluorescent using FACS technology. **b**, The measured cells were divided into 6 individual clusters based on gene expression profiles using UMAP. **c-h**, The violin plots of some endothelial cell marker genes. **i**, The proportion of ECs in each cluster of control and high glucose groups. **j**, Changes of ECs percentage in arterial and capillary ECs, endocardium, and proliferating ECs of control and high glucose group.

Figure 5 Foxo1a was involved in the excessive angiogenesis induced by high glucose treatment. a, The volcano plot of differential expression genes in arterial and capillary ECs. The avg_log2FC greater than 1 was considered significant, including 523 down-regulated genes (blue dots) and 1201 up-regulated genes (red dots). **b**, GO analysis of 523 down-regulated genes in arterial and capillary ECs. **c,** The feature plot of ECs marker gene pecam1 of control and high glucose group in arterial and capillary ECs. **c',** The violin plot of ECs marker gene pecam1 of control and high glucose group in arterial and capillary ECs. **d**, The

feature plot of gene foxo1a of control and high glucose group in arterial and capillary ECs. **d',** The violin plot of gene foxo1a of control and high glucose group in arterial and capillary ECs. **e**, Average expression of gene pecam1 and foxo1a in control and high glucose group. **f**, Whole-mount in situ hybridization analysis of foxo1a in control, high glucose, and high L-glucose treated embryos. **g**, A diagram showing the foxo1 inhibitor treatment time window. **h**, Confocal imaging analysis of control embryos, AS1842856 treated embryos and foxo1a MO-injected embryos. Arrowheads indicate ectopic angiogenic sprouts. **i**, Statistical analysis of the total length of ISVs in control embryos, AS1842856 treated embryos, and foxo1a MO-injected embryos. *t-test*, ****p<0.0001.

Figure 6 Foxo1a gain of function can partially rescue the excessive angiogenesis induced by high glucose treatment. a, A diagram showing the high glucose treatment time window and heat shock treated time point. **b**, Confocal imaging analysis of blood vessels in control *Tg(fli1aEP:EGFP-CAAX)*^{ntu666} embryos. **c,** Confocal imaging analysis of blood vessels in high glucose treated *Tg(fli1aEP:EGFP-CAAX)*^{ntu666} embryos. **d-d'**, Confocal imaging analysis of blood vessels in *hsp70l:foxo1a-P2A-mCherry* and high glucose treated *Tg(fli1aEP:EGFP-CAAX)*^{ntu666} embryos. **e**, Statistical analysis of the total length of ISVs in control, high glucose-treated, *hsp70l:foxo1a-P2A-mCherry* and high glucose treated embryos, respectively. one-way ANOVA, ****p<0.0001. **f**, A diagram showing the high glucose treatment time window and imaging time point. **g**, Confocal imaging analysis of blood vessels in high glucose treated *Tg(fli1aEP:EGFP-CAAX)*^{ntu666} embryos. **h**, Confocal imaging analysis of blood vessels in *fli1EP:foxo1a-mApple* and high glucose treated

Tg(fli1aEP:EGFP-CAAX)^{ntu666} embryos. **i**, Statistical analysis of the number of sprouts per ISV in high glucose treated embryos, and *fli1EP:foxo1a-mApple* & high glucose treated embryos. *t-test*, ****p<0.0001. **j,** Statistical analysis of the total length of ISVs in high glucose treated embryos, and *fli1EP:foxo1a-mApple* & high glucose treated embryos. *t-test*, ***p<0.001.

Figure 7 Marcksl1a over-expression induced excessive angiogenesis in zebrafish embryos. a, The violin plot of ECs marker gene kdrl of control and high glucose group in arterial and capillary ECs. **b**, The violin plot of gene *marcksl1a* of control and high glucose group in arterial and capillary ECs. **c,** Real-rime PCR analysis of *marcksl1a* expression in control, high glucose, and high L-glucose treated embryos. *t-test*, ****p<0.0001. **d**, Whole-mount in situ hybridization analysis of *marcksl1a* in control, high glucose, and high L-glucose treated embryos. **e-f'**, Confocal imaging analysis of blood vessels in control and *hsp70l:marcksl1a-P2A-mCherry* injected *Tg(fli1aEP:EGFP-CAAX)*^{ntu666} embryos. **g**, Statistical analysis of the total length of ISVs in control and *hsp70l:marcksl1a-P2A-mCherry* injected embryos. *t-test*, **p<0.01.

Figure 8 Noncaloric monosaccharides induced excessive angiogenesis through foxo1a-marcksl1a signal in zebrafish embryos. a, A diagram showing the Foxo1 inhibitor and heat shock treatment time window. **b**, Real-rime PCR analysis of *marcksl1a* expression in control and AS1842856 treated embryos. *t-test*, ***p<0.001. **c**, Real-rime PCR analysis of *marcksl1a* expression in control and *foxo1a* overexpressed embryos. *t-test*, **p<0.01. **d,** A sequence

logo of Foxo1 binding sequence presented in the JASPAR database (https://jaspar.genereg.net/) and two candidate binding sites at the upstream of transcription start site (TSS) of *marcksl1a* in zebrafish. **e,** Results of the ChIP-PCR assay indicated that BS1 and BS2 are Foxo1a-binding sites of *marcksl1a* in zebrafish. Input sonicated genomic DNA samples without immunoprecipitation as a positive control. IgG, sonicated, and IgG-immunoprecipitated genomic DNA samples as a negative control. **f-g**, Luciferase reporter activity in *foxo1a* overexpressed or knocked down embryos, respectively. *t-test*, $^{**}p<0.01$, $^{****}p<0.0001$. **h-m,** Confocal imaging analysis of blood vessels in control, high glucose, high glucose & Lenvatinib, high glucose+*marcksl1a* MO, high L-glucose and high L-glucose+*marcksl1a* MO groups. **n**, Statistical analysis of the total length of ISVs in the groups in figure h-m, respectively. one-way ANOVA, $^{****}p<0.0001$.

Supplementary Figure Legends

Supplementary Figure 1 Confocal imaging analysis of *Tg(fli1aEP:EGFP-CAAX)^{ntu666}* embryos at 48 hpf (a) and 3 dpf (b).

Supplementary Figure 2 The diagrams show the glucose treatment time window and imaging time point.

Supplementary Figure 3 Total glucose concentrations at different development stages in control and high glucose treated embryos. **a**, A diagram showing the glucose treatment time window and concentration measuring time point. **b**, Statistical analysis of the glucose concentration in control and high glucose-treated embryos. one-way ANOVA, ****p<0.0001.

Supplementary Figure 4 Stereo microscopic analysis of control, glucose, and sucrase-treated embryos in a bright field. a-c, Imaging analysis of control, glucose, and sucrase treated embryos in bright field. **d**, A diagram showing the sucrase treatment time window and imaging time point. **e**, A diagram indicating the imaging positions of the zebrafish embryos. **f,** Confocal imaging analysis of the control and sucrase treated *Tg(fli1aEP:EGFP-CAAX)^{ntu666}* embryos. The red bar indicates position 1; the green bar indicates the position. **g**, A diagram showing the sucrase treatment time window and imaging time point. **h**, Confocal imaging analysis of the control and sucrase treated *Tg(fli1aEP:EGFP-CAAX)^{ntu666}* embryos. The red bar indicates position 1; the green bar indicates the position.

Supplementary Figure 5 Confocal imaging analysis of 1%—4% glucose-treated blood vessels. a, A diagram showing the glucose treatment time window and imaging time point. **b-g'**, Confocal imaging analysis of the control, 1%, 2%, 3%, and 4% glucose-treated *Tg(fli1aEP:EGFP-CAAX)*^{ntu666} embryos.

Supplementary Figure 6 Fructose treatment caused excessive angiogenesis in zebrafish. a, A diagram showing the fructose treatment time window and imaging time point. **b**, A diagram indicating the imaging position of the zebrafish embryos. **c-d**, Confocal imaging analysis of the control and glucose-treated *Tg(fli1aEP:EGFP-CAAX)*^{ntu666} embryos. e-f, Imaging analysis of control and fructose treated embryos in bright field.

Supplementary Figure 7 Lactose and maltose treatment did not cause excessive angiogenesis in zebrafish. a, A diagram showing the lactose and maltose treatment time window and imaging time point. **b-d"**, Confocal imaging analysis of the control, lactose, and maltose treated *Tg(fli1aEP:EGFP-CAAX)*^{ntu666} embryos.

Supplementary Figure 8 Higher concentration sucrase and maltose treatment cause excessive angiogenesis in zebrafish embryos. a, A diagram showing the sucrase and maltose treatment time window and imaging time point. **b,** Confocal imaging analysis of the control and sucrase treated *Tg(fli1aEP:EGFP-CAAX)*^{ntu666} embryos. **c,** Statistical analysis of the total length of ISVs in control and sucrase-treated embryos. *t-test*, ****p<0.0001.**d,**

Confocal imaging analysis of the control and maltose-treated *Tg(fli1aEP:EGFP-CAAX)*^{ntu666} embryos.

Supplementary Figure 9 Pyruvic acid treatment did not cause excessive angiogenesis in zebrafish. a, A diagram showing the pyruvic acid treatment time window and imaging time point. **b**, Confocal imaging analysis of the pyruvic acid-treated *Tg(fli1aEP:EGFP-CAAX)*^{ntu666} embryos. **c**, A diagram showing the pyruvic acid treatment time window and imaging time point. **d**, Confocal imaging analysis of the pyruvic acid-treated *Tg(fli1aEP:EGFP-CAAX)*^{ntu666} embryos.

Supplementary Figure 10 Overview of the number of genes, total UMIs, and percentage of mitochondrial UMIs for the single-cell RNA sequencing. a, Before filtering. **b**, After filtering. Cell selection criteria: 500< number of genes < 3000; 0< percentage of mitochondrial UMIs < 5%.

Supplementary Figure 11 UMAP representation of EC subpopulations. All single cells (after filtering) from the control and D-glucose treated were included in this illustration.

Supplementary Figure 12 Transcriptome sequencing analysis of control, high D-glucose, and high L-glucose treated embryos. a, The heatmap of differentially expressed genes (DEGs). **b**, Volcano map of DEGs after high D-glucose treatment. **c,** Volcano map of DEGs after high L-glucose treatment.

Supplementary Figure 13 The heatmap of metabolism-related genes. a, The heatmap of gluconeogenesis-related genes. **b**, The heatmap of glycolysis-related genes. **c**, The heatmap of oxidative phosphorylation-related genes.

Supplementary Figure 14 Multiple amino acid sequence alignment of mouse FOXO1 and zebrafish Foxo1a. The DNA binding domain of mouse FOXO1 is demarcated with blue.

Supplementary Figure 15 Confocal imaging analysis of blood vessels in the embryos with Lenvatinib treatment. a, A diagram showing the Lenvatinib treatment time window and imaging time point. **b**, Confocal imaging analysis of the control and Lenvatinib treated *Tg(fli1aEP:EGFP-CAAX)*^{ntu666} embryos. **c**, A diagram showing the Lenvatinib treatment time window and imaging time point. **d**, Confocal imaging analysis of the control and Lenvatinib treated *Tg(fli1aEP:EGFP-CAAX)*^{ntu666} embryos.

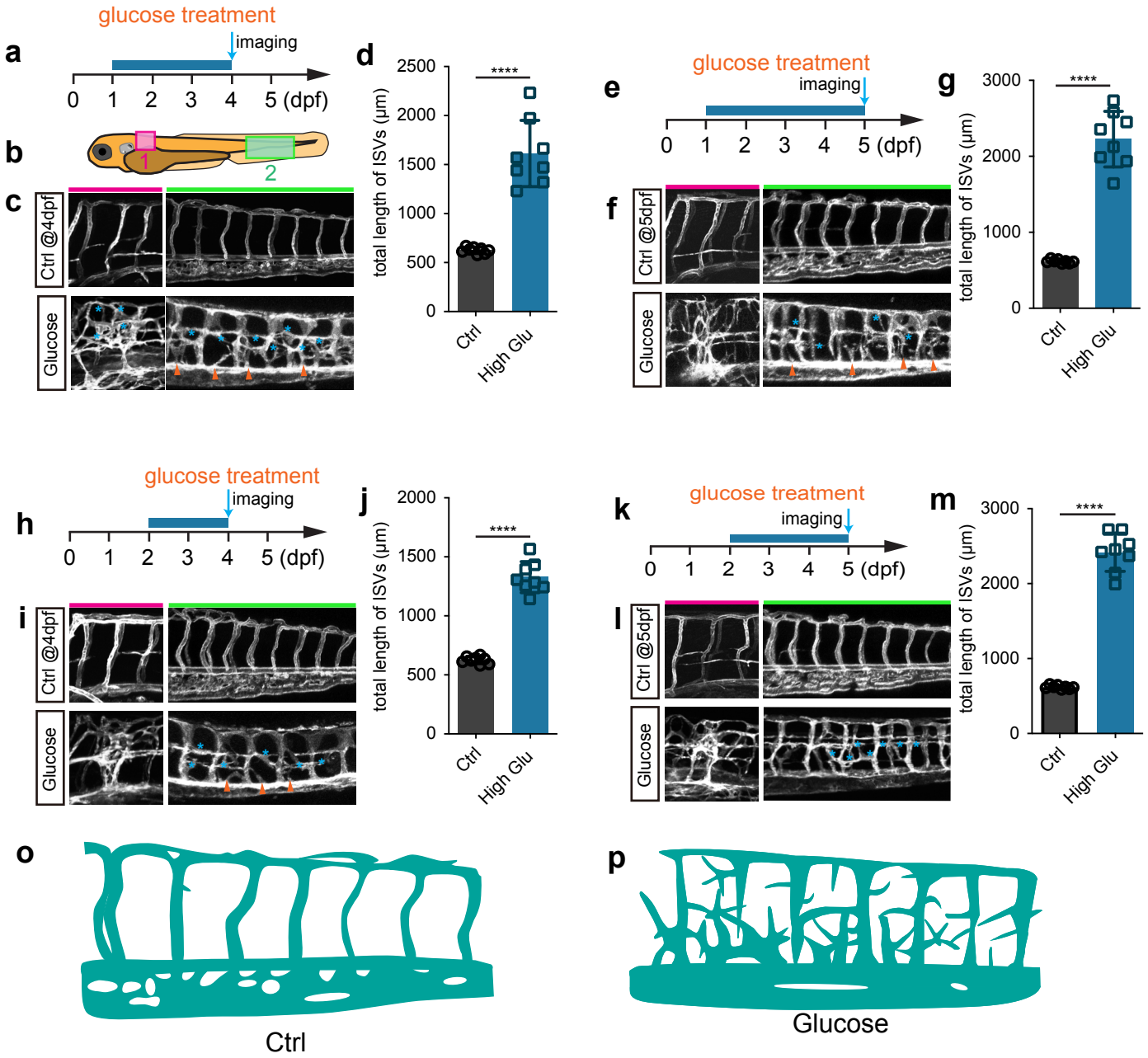
a
glucose treatment
imaging
0 1 2 3 4 5 (dpf)
b
1
2
c
Ctrl @4dpf
Glucose
d
total length of ISVs (μm)
2500
2000
1500
1000
500
0
****
Ctrl
High Glu
e
glucose treatment
imaging
0 1 2 3 4 5 (dpf)
f
Ctrl @5dpf
Glucose
g
total length of ISVs (μm)
3000
2000
1000
0
****
Ctrl
High Glu
h
glucose treatment
imaging
0 1 2 3 4 5 (dpf)
i
Ctrl @4dpf
Glucose
j
total length of ISVs (μm)
2000
1500
1000
500
0
****
Ctrl
High Glu
k
glucose treatment
imaging
0 1 2 3 4 5 (dpf)
l
Ctrl @5dpf
Glucose
m
total length of ISVs (μm)
3000
2000
1000
0
****
Ctrl
High Glu
o
Ctrl
p
Glucose

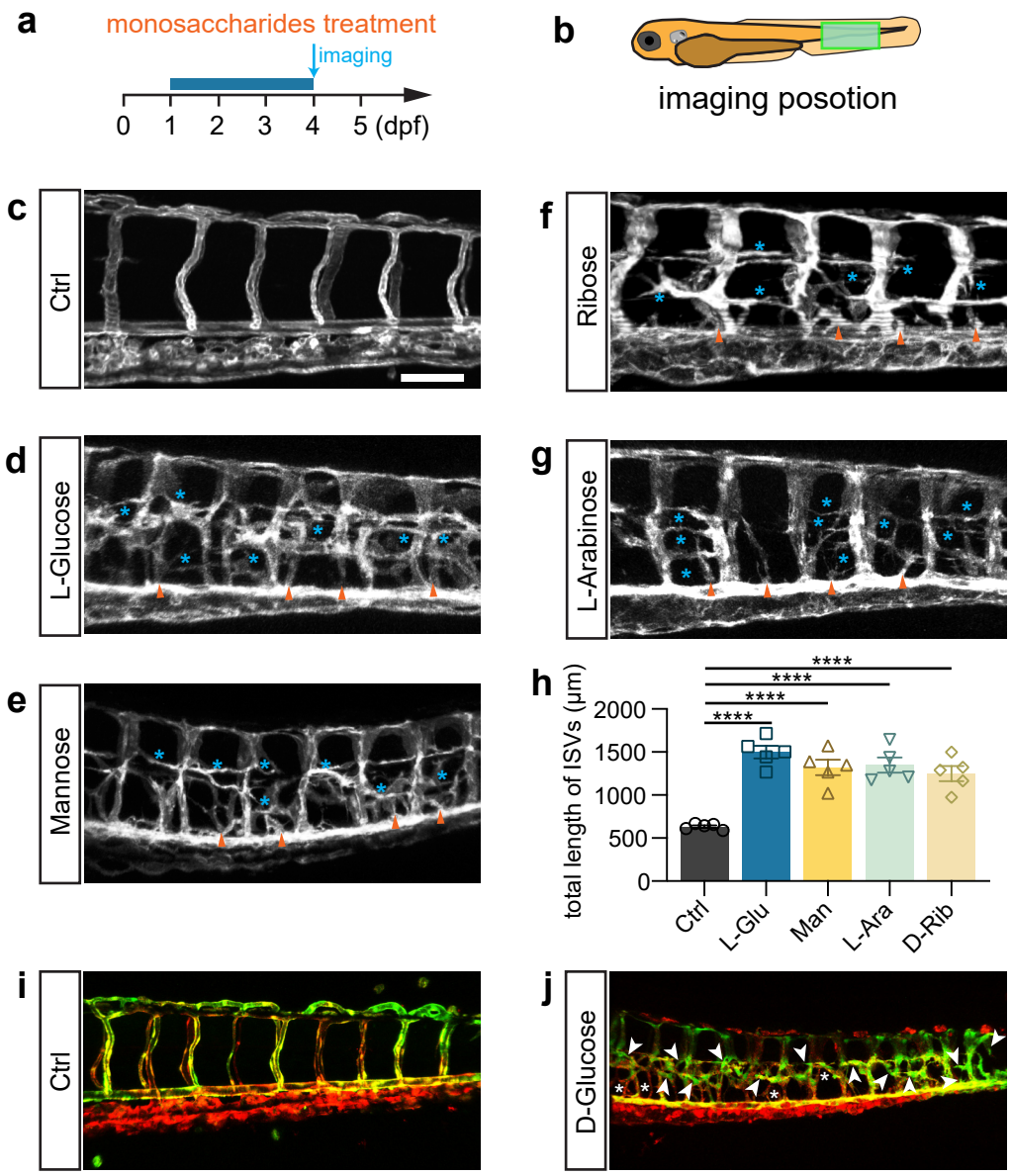
a
monosaccharides treatment
imaging
0 1 2 3 4 5 (dpf)
b
imaging posotion
c
Ctrl
d
L-Glucose
e
Mannose
f
Ribose
g
L-Arabinose
h
total length of ISVs (μm)
2000
1500
1000
500
0
****
****
****
****
Ctrl
L-Glu
Man
L-Ara
D-Rib
i
Ctrl
j
D-Glucose

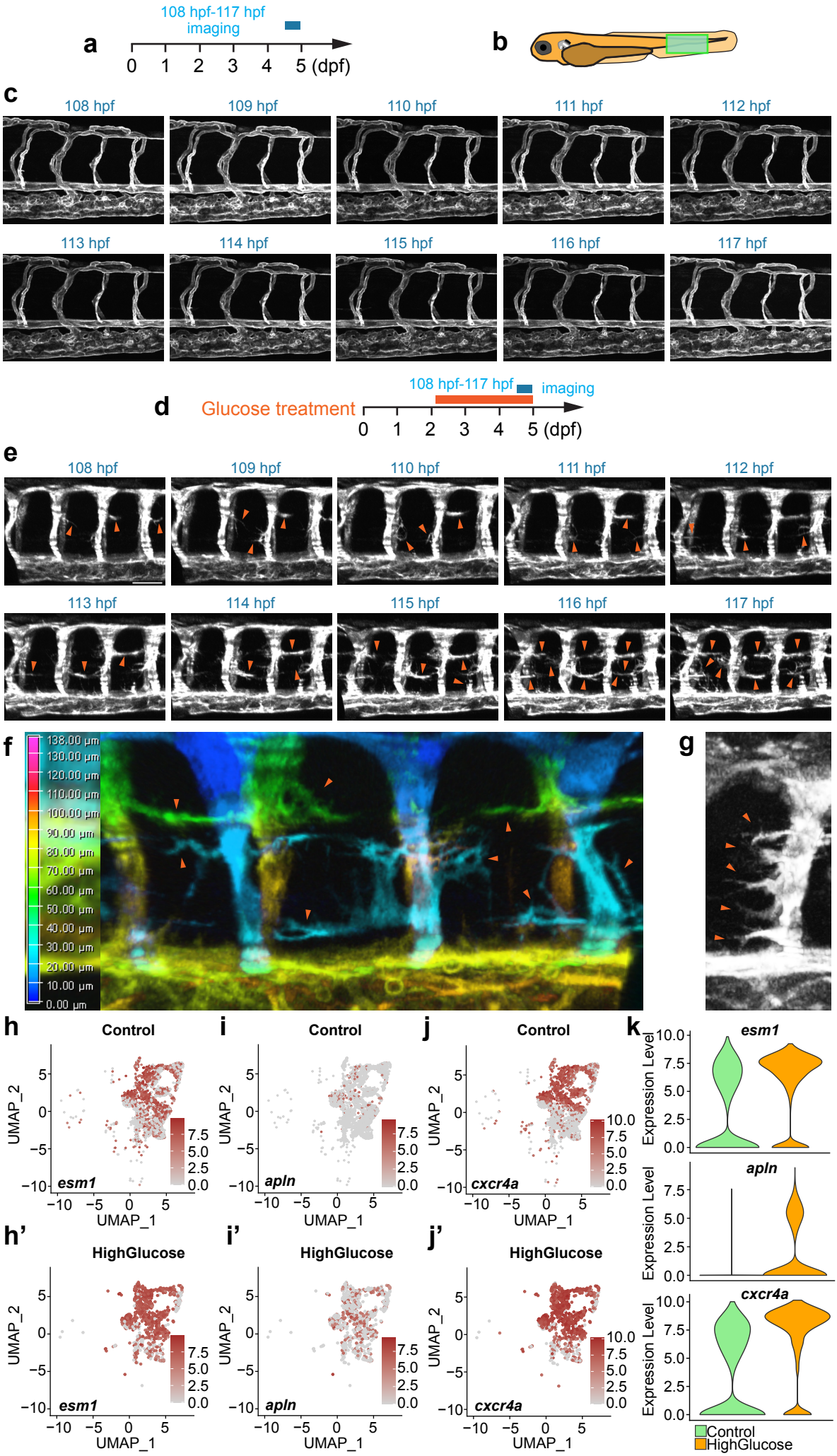
a
108 hpf-117 hpf
imaging
0 1 2 3 4 5 (dpf)
b
c
108 hpf
109 hpf
110 hpf
111 hpf
112 hpf
113 hpf
114 hpf
115 hpf
116 hpf
117 hpf
d
Glucose treatment
108 hpf-117 hpf
imaging
0 1 2 3 4 5 (dpf)
e
f
138.00 µm
130.00 µm
120.00 µm
110.00 µm
100.00 µm
90.00 µm
80.00 µm
70.00 µm
60.00 µm
50.00 µm
40.00 µm
30.00 µm
20.00 µm
10.00 µm
0.00 µm
g
h
Control
esm1
UMAP_2
UMAP_1
i
Control
apln
j
Control
cxcr4a
k
esm1
apln
cxcr4a
Expression Level
h'
HighGlucose
i'
HighGlucose
j'
HighGlucose
Control
HighGlucose

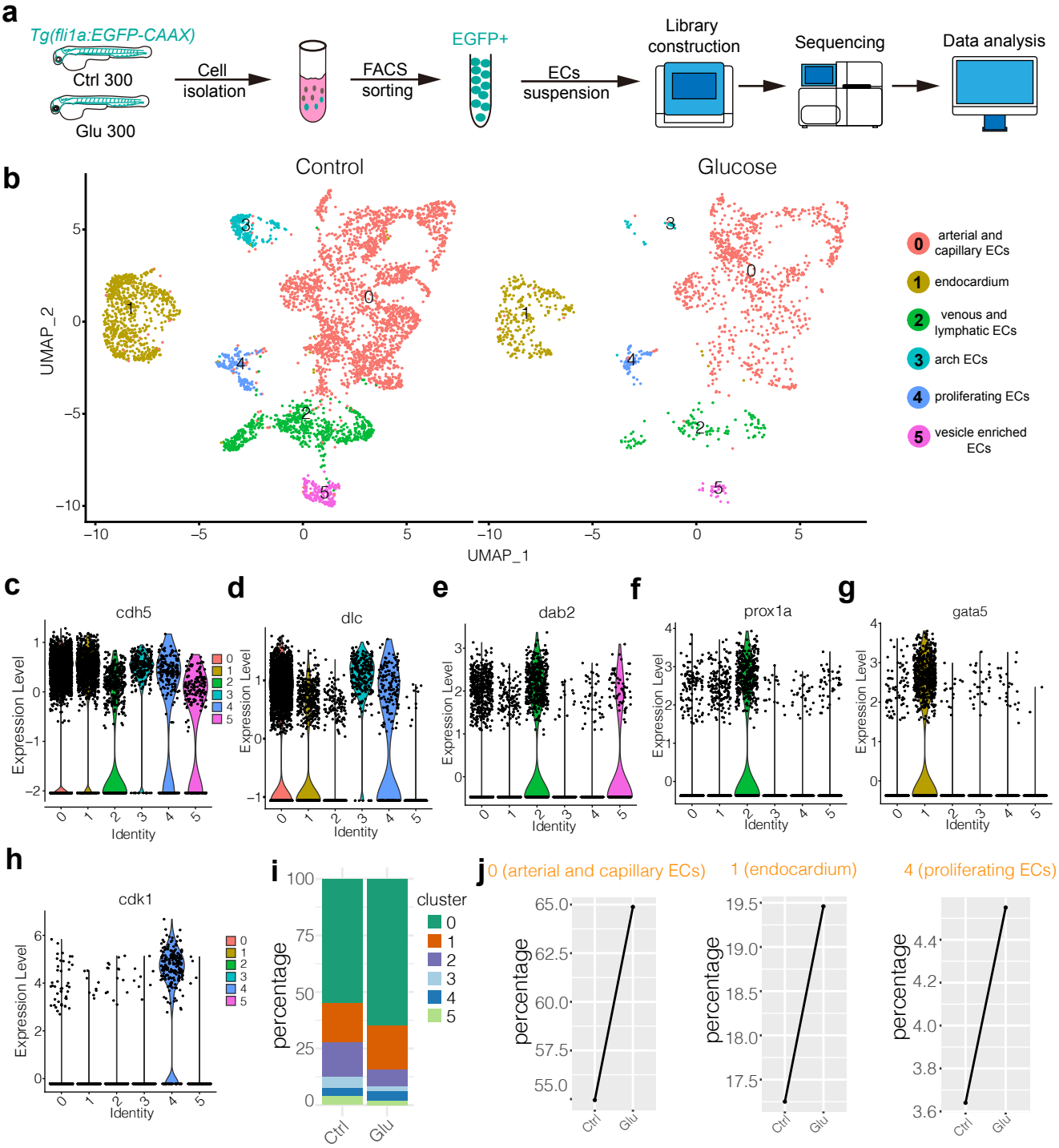
a
Tg(fli1a:EGFP-CAAX)
Ctrl 300
Glu 300
Cell isolation
FACS sorting
EGFP+
ECs suspension
Library construction
Sequencing
Data analysis
b
Control
Glucose
UMAP_2
UMAP_1
0 arterial and capillary ECs
1 endocardium
2 venous and lymphatic ECs
3 arch ECs
4 proliferating ECs
5 vesicle enriched ECs
c
cdh5
d
dlc
e
dab2
f
prox1a
g
gata5
Expression Level
Identity
h
cdk1
i
percentage
cluster
Ctrl
Glu
j
0 (arterial and capillary ECs)
1 (endocardium)
4 (proliferating ECs)
percentage

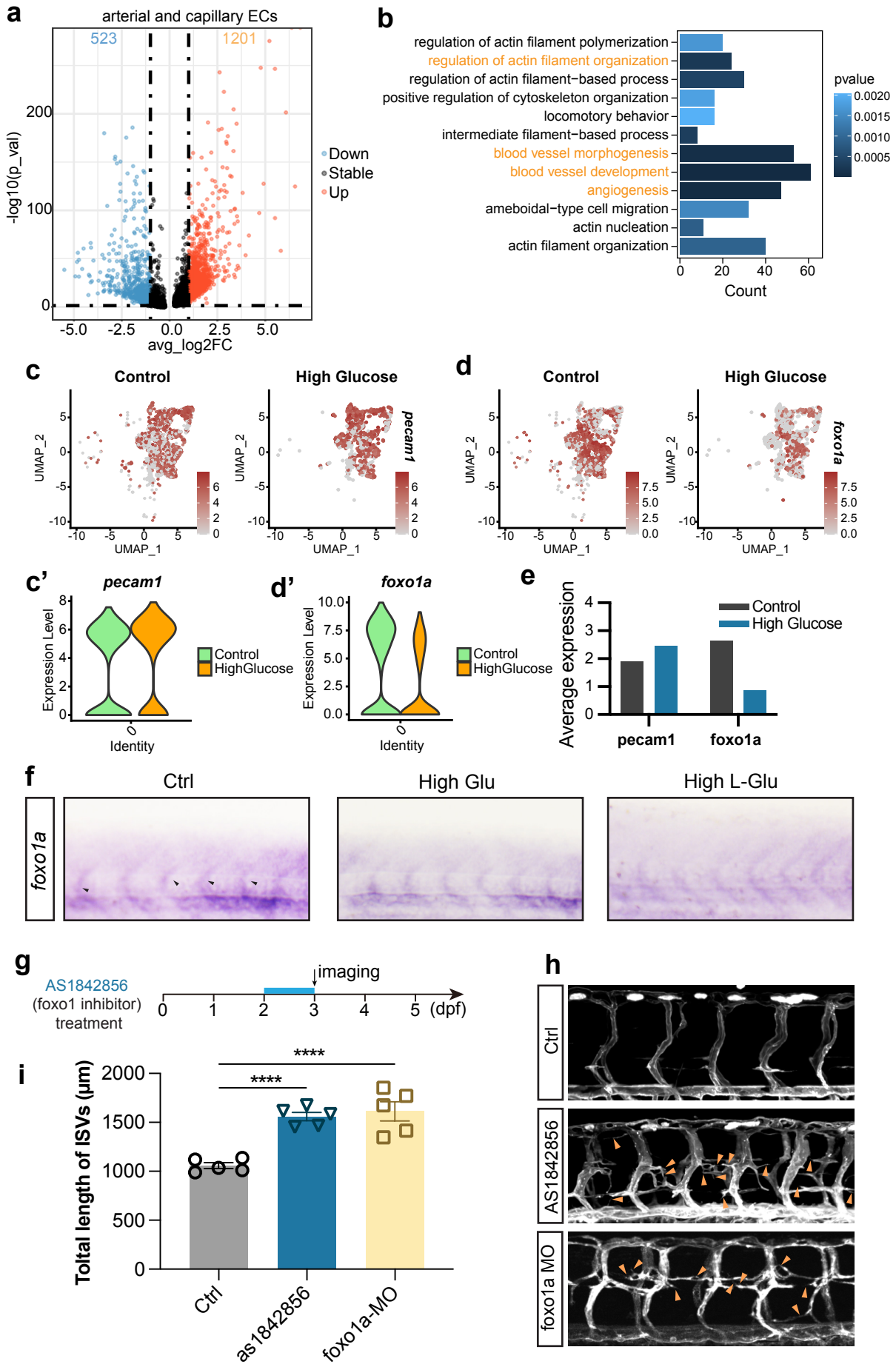
a
arterial and capillary ECs
523
1201
-log10(p_val)
avg_log2FC
Down
Stable
Up
b
regulation of actin filament polymerization
regulation of actin filament organization
regulation of actin filament−based process
positive regulation of cytoskeleton organization
locomotory behavior
intermediate filament−based process
blood vessel morphogenesis
blood vessel development
angiogenesis
ameboidal−type cell migration
actin nucleation
actin filament organization
Count
pvalue
c
Control
High Glucose
pecam1
UMAP_1
UMAP_2
d
Control
High Glucose
foxo1a
c'
pecam1
Expression Level
Identity
Control
HighGlucose
d'
foxo1a
e
Average expression
Control
High Glucose
pecam1
foxo1a
f
Ctrl
High Glu
High L-Glu
foxo1a
g
AS1842856
(foxo1 inhibitor)
treatment
imaging
(dpf)
h
Ctrl
AS1842856
foxo1a MO
i
Toltal length of ISVs (μm)
****
****
Ctrl
as1842856
foxo1a-MO

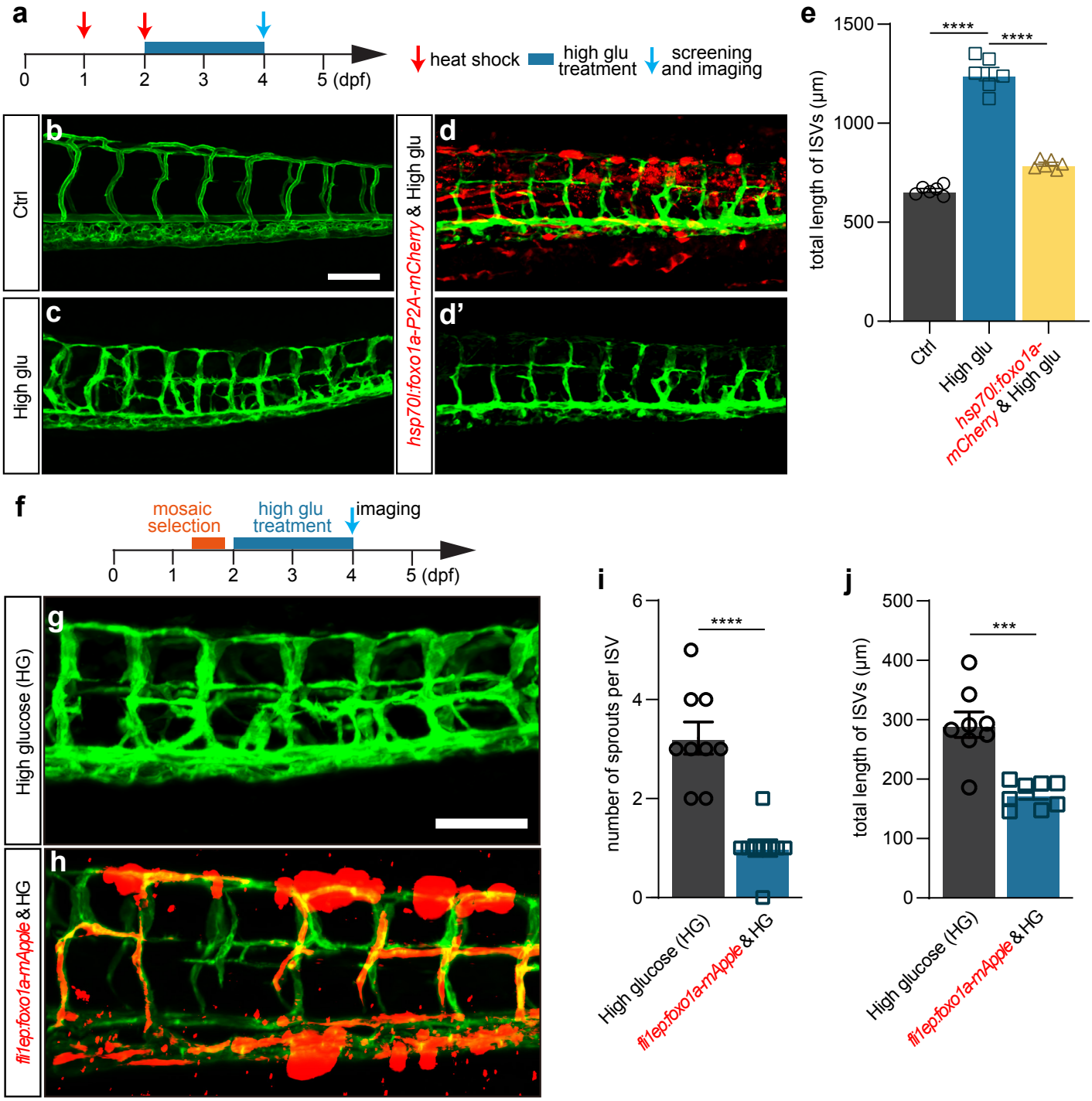
a
0
1
2
3
4
5 (dpf)
heat shock
high glu treatment
screening and imaging
Ctrl
High glu
b
c
d
d'
hsp70l:foxo1a-P2A-mCherry & High glu
e
total length of ISVs (µm)
1500
1000
500
0
****
****
Ctrl
High glu
hsp70l:foxo1a-mCherry & High glu
f
mosaic selection
high glu treatment
imaging
0
1
2
3
4
5 (dpf)
High glucose (HG)
fli1ep:foxo1a-mApple & HG
g
h
i
number of sprouts per ISV
6
4
2
0
****
High glucose (HG)
fli1ep:foxo1a-mApple & HG
j
total length of ISVs (µm)
500
400
300
200
100
0
***
High glucose (HG)
fli1ep:foxo1a-mApple & HG

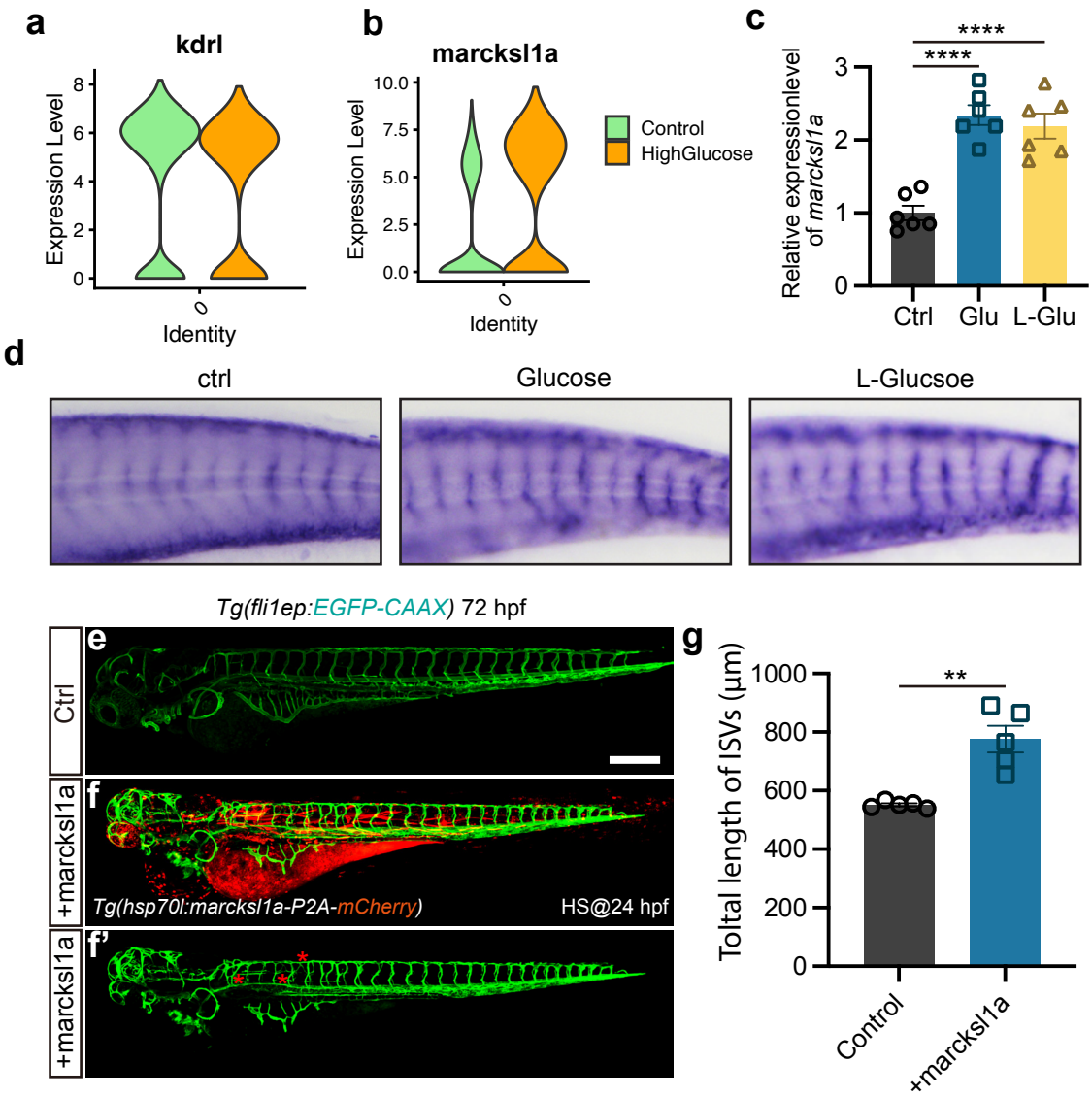
a
kdrl
Expression Level
Identity
b
marcksl1a
Expression Level
Identity
Control
HighGlucose
c
Relative expressionlevel of marcksl1a
****
****
Ctrl
Glu
L-Glu
d
ctrl
Glucose
L-Glucsoe
Tg(fli1ep:EGFP-CAAX) 72 hpf
Ctrl
+marcksl1a
+marcksl1a
e
f
f'
Tg(hsp70l:marcksl1a-P2A-mCherry)
HS@24 hpf
g
Toltal length of ISVs (μm)
**
Control
+marcksl1a

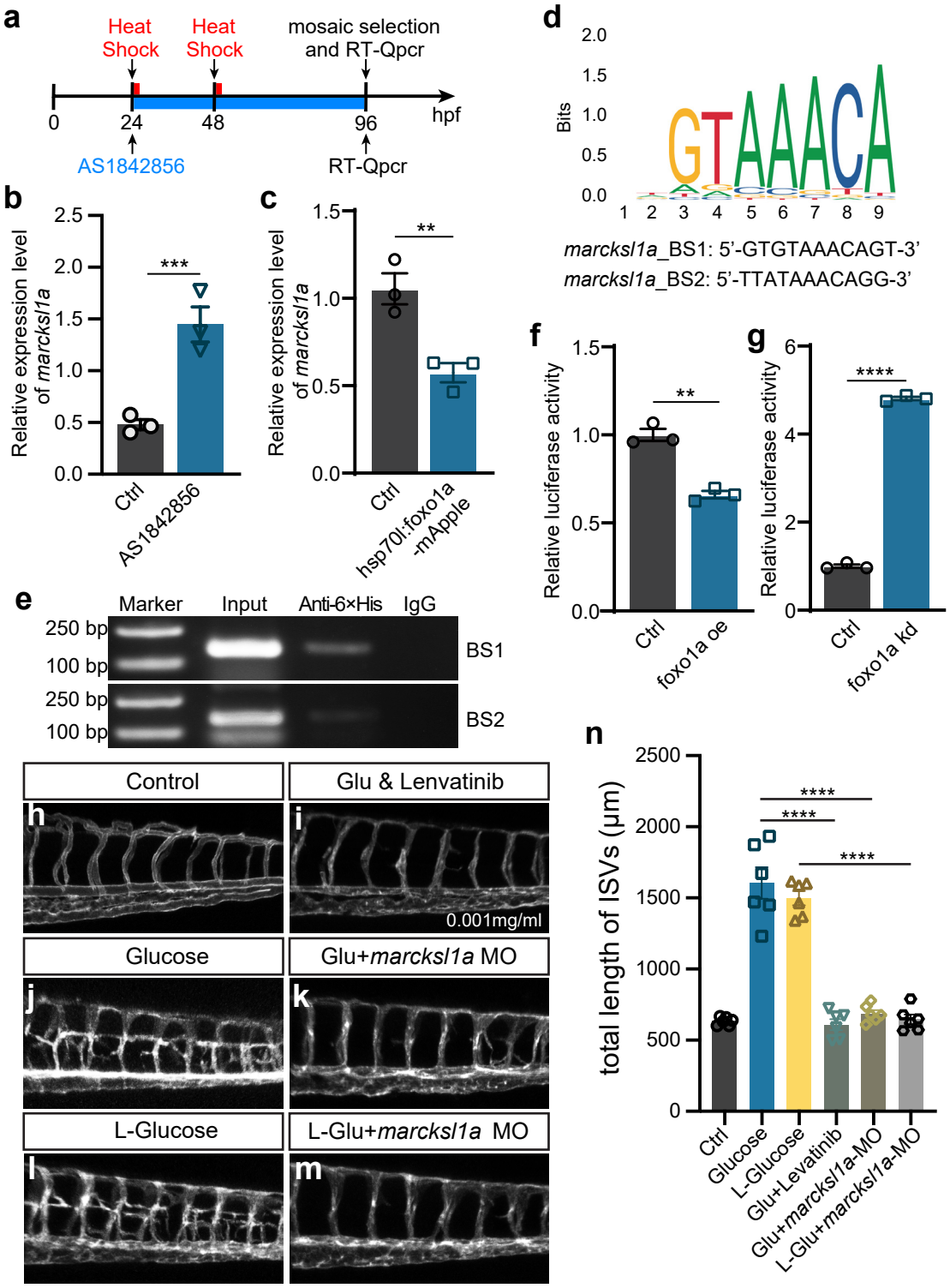
a
Heat Shock
Heat Shock
mosaic selection and RT-Qpcr
0
24
48
96
hpf
AS1842856
RT-Qpcr
b
Relative expression level of marcksl1a
Ctrl
AS1842856
c
Relative expression level of marcksl1a
Ctrl
hsp70l:foxo1a -mApple
d
Bits
marcksl1a_BS1: 5'-GTGTAAACAGT-3'
marcksl1a_BS2: 5'-TTATAAACAGG-3'
e
Marker
Input
Anti-6×His
IgG
250 bp
100 bp
BS1
BS2
f
Relative luciferase activity
Ctrl
foxo1a oe
g
Relative luciferase activity
Ctrl
foxo1a kd
Control
Glu & Lenvatinib
0.001mg/ml
Glucose
Glu+marcksl1a MO
L-Glucose
L-Glu+marcksl1a MO
n
total length of ISVs (μm)
Ctrl
Glucose
L-Glucose
Glu+Levatinib
Glu+marcksl1a-MO
L-Glu+marcksl1a-MO